Suppression of the critical thickness threshold for conductivity at the LaAlO3/SrTiO3 interface

E. Lesne, N. Reyren, D. Doennig, R. Mattana, F. Choueikani, H Jaffrès, V. Cros, F. Petroff, P. Ohresser, R. Pentcheva, et al.

Suppression of the Critical Thickness Threshold for Conductivity at the $LaAlO_3/SrTiO_3$ Interface

E. Lesne,[1,*] N. Reyren,[1] D. Doennig,[2] R. Mattana,[1] F. Choueikani,[3] H. Jaffrès,[1]
V. Cros,[1] F. Petroff,[1] P. Ohresser,[3] R. Pentcheva,[2] A. Barthélémy,[1] and M. Bibes[1]

[1] *Unité Mixte de Physique CNRS-Thales, 1 Av. A. Fresnel, 91767 Palaiseau, France and Université Paris-Sud, 91405 Orsay, France*

[2] *Department of Earth and Environmental Sciences, Section Crystallography and Center of Nanoscience (CENS), University of Munich, Theresienstrasse 41, DE-80333 Munich, Germany*

[3] *Synchrotron SOLEIL, L'Orme des Merisiers, Saint-Aubin, BP 48, FR-91192 Gif sur Yvette, France*

[*] edouard.lesne@thalesgroup.com

Due to the matching of their pseudo-cubic unit cell and the large variety of available ground states, perovskite materials engineered in epitaxial heterostructures have triggered a wide range of investigations over the last decade. The interface formed by an $LaAlO_3$ thin film grown on top of a TiO_2-terminated $SrTiO_3$ substrate which hosts a two-dimensional electronic system has become the prototypical example of this new field of interest. Although controversy exists regarding some of its physical properties and their precise origin, it is universally found that conductivity only appears beyond an $LaAlO_3$ thickness threshold of four unit cells. Here, through magnetotransport and X-ray absorption spectroscopy experiments, we show that this critical thickness can be reduced to just one unit cell when a metallic film of cobalt is deposited on top of $LaAlO_3$. First-principles calculations indicate that Co modifies the electrostatic boundary conditions and induces charge transfer toward the Ti $3d$ bands, therefore supporting the electrostatic origin of the electronic system at the $LaAlO_3/SrTiO_3$ interface. Our results expand the interest of this low-dimensional oxide system from in-plane to perpendicular transport and to the exploration of elastic and inelastic tunnel-type transport of (spin-polarized) carriers.

Combined in heterostructures, oxide thin films offer a new playground with virtually unlimited combinations to realize artificial systems and to explore emerging phenomena absent in bulk compounds[1]. Ohtomo and Hwang's 2004 striking discovery of conducting $LaAlO_3/SrTiO_3$ heterointerfaces has fast-tracked this system as the fruit fly for such investigations[2]. The $LaAlO_3/SrTiO_3$ system exhibits gate-tunable quasi-two dimensional electronic conduction[3], Rashba spin-orbit interaction[4,5] and superconductivity[6–8], displays indications of magnetism[9,10] and even close coexistence of the latter two[11–13]. This makes the $LaAlO_3/SrTiO_3$ system attractive for fundamental studies as well as promising for potential applications such as oxide-based electronics[14–16].

While the perovskite crystals $LaAlO_3$ (LAO) and $SrTiO_3$ (STO) are both wide band-gap insulators, the growth of an epitaxial LAO film on a TiO_2-terminated, (001)-oriented STO substrate leads to an insulator-to-metal transition when the LAO thickness reaches 4 unit cells[3]. Due to their ionic nature, the STO(001) substrate (non-polar) and the LAO(001) film (polar) form a strongly polar interface. This results in an increasing electrostatic potential as the LAO thickness is increased, leading to an electronic reconstruction with charge transferred toward the STO top TiO_2 subplane[17].

Recently, first-principles calculations predicted a conductive system at the LAO/STO interface for heterostructures with various metallic capping layers, and an LAO thickness of 2 uc[18]. In this Letter, we present results of electrical magnetotransport and X-ray absorption spectroscopy (XAS) experiments on LAO/STO samples with either bare LAO surfaces or a metallic capping layer of cobalt, combined with density functional theory (DFT) calculations. We demonstrate the existence of metallic conductivity on the STO side for an LAO thickness as thin as 1 unit cell (uc).

RESULTS

Magnetotransport measurements of Co/LAO/STO samples.

LAO films were grown by pulsed laser deposition on TiO_2-terminated STO(001) substrates and followed by *in situ* magnetron sputtering deposition of a 2 to 2.5 nm cobalt thin film, capped with a 3 nm AlO_x layer to prevent Co

oxidation. Details of the samples fabrication can be found in the Methods section.

The unpatterned samples were electrically contacted with aluminum wires by ultrasonic wedge bonding. Four-point transport measurements (longitudinal R_{xx} and transverse R_{xy} magnetoresistances) were performed by connecting the corners of the square sample in the van der Pauw geometry. Figure 1(a) shows R_{xx} *vs.* temperature for Co/LAO/STO heterostructures with various LAO thicknesses, and a Co/STO control sample for which the STO substrate experienced the same procedure of thermal and oxygen pressure cycles as for the LAO/STO samples. While the Co/STO sample shows very little variation of its resistance (less than one percent) across the explored temperature range, the Co-capped LAO/STO samples display a strong reduction of their resistance as temperature is decreased, which readily suggests that the LAO/STO interface conducts, even for samples with an LAO film thickness smaller than 4 uc.

Following these observations, we now model the Co/LAO($n \geq$1 uc)/STO heterostructures by two conducting layers in parallel composed of the Co overlayer and the STO sublayer. According to this simple picture, and supposing a temperature-independent resistance of the Co capping layer [see Fig. 1(a)], the temperature evolution of the STO sublayer's longitudinal resistance is given by:

$$R_{xx}^{STO}(T) = \frac{R_{xx}^{Co} \cdot R_{xx}^{meas}(T)}{R_{xx}^{Co} - R_{xx}^{meas}(T)}. \quad (1)$$

The sheet resistance of the STO sublayer is defined as $R_{\square}^{STO} = R_{xx}^{STO}(T) \times \frac{\pi}{ln(2)}$, assuming a homogeneous conductance in the geometry of the inset of Fig. 1(a)[19], supported by the fact that $R_{xx} \approx R_{yy}$ within a few percent. For each sample we calculate $R_{xx}^{STO}(T)$ by taking the data set as $R_{xx}^{meas}(T)$, and R_{xx}^{Co} as the measured value at room temperature [R_{xx}^{Co}=R_{xx}^{meas}(290K)] for the corresponding sample. Figure 1(b) displays the calculated sheet resistance $R_{\square}^{STO}$ of the Co/LAO/STO samples in the low temperature range (below 100 K).

Next we focus on transport experiments carried out in Hall configuration at room temperature and at low temperature (1.4 K). The measured transverse magnetoresistance curves were antisymmetrized ($R_{xy}(H) = [R_{xy}^{meas}(H) - R_{xy}^{meas}(-H)]/2$). Antisymmetrized traces $R_{ac-db}(H)$ and $R_{db-ca}(H)$ appear indistinguishable on Fig. 2(a,b), suggesting again good sample homogeneity and no artefacts due to the data analysis. In the case of the LAO(4 uc)/STO sample, Hall measurements taken at room temperature show a linear behavior for magnetic field up to 4 T [see Fig. 2(a)] with an extracted sheet carrier densitiy $n_{\square} = 6.4 \times 10^{13}$ cm^{-2}. In contrast, Co/STO and Co/LAO/STO samples exhibit at room temperature a Hall effect dominated by the cobalt layer, independent of the LAO thickness [see inset of Fig. 2(a)], with a low magnetic field regime ($|\mu_0 H| \leq 1.5$ T) displaying the anomalous Hall effect (AHE) characteristic of a ferromagnetic metal. In the high field regime ($|\mu_0 H| \geq 2$ T), the Co magnetization is rotated out of plane and the Co-capped samples exhibit a normal Hall effect with a weak negative slope of order -10 mΩ/T (*i.e.* $\sim 10^{23} e{\cdot}$cm^{-3}).

Figure 2(b) displays Hall data acquired at 1.4 K. $R_{xy}(H)$ measured at 1.4 K in Co/STO shows essentially no change when compared to room temperature measurements [see insets of Fig. 2(a,b)]. On the other hand, $R_{xy}(H)$ behavior of Co/LAO(n=1,2,4 uc)/STO samples at 1.4 K display striking similarities with those carried out on uncapped LAO(4 uc)/STO samples. The Hall resistance trace of the LAO(4 uc)/STO sample is not perfectly linear at 1.4 K, a behavior believed to arise from the multi-band structure of STO[20–22]. Evidence for this is given from the DFT calculations in the Supplementary Information Fig. S3. We only consider the 'high field' regime ($|\mu_0 H| \geq 3$ T) where $n_{\square}$, the total electron density in the STO, is given by $n_{\square} = -\frac{1}{|e| \cdot R_H}$, with e the elementary charge and R_H the Hall coefficient determined for $|\mu_0 H| \geq 3$ T. The kink observed in the LAO(4 uc)/STO Hall trace $R_{xy}(H)$ is well

reproduced in Co capped LAO samples at 1.4 K, regardless of the LAO thickness. This close resemblance for both sets of samples suggests a common host for the observed electronic transport. The measured Hall coefficients, and related carrier densities show no correlation with LAO thickness. Taking the sheet resistance and Hall coefficient at 1.4 K, one can estimate the electronic mobility $\mu_H^{STO} = R_H/R_\square^{STO}$ of the STO sublayer in Co/LAO/STO samples. Values in the range of $1 - 6 \times 10^2$ cm^2/(V·s) are found. We note that the Co layer is not expected to play a role in Hall effect measurements at 1.4 K, due to its much lower mobility [μ_H^{Co} <1 cm^2/(V·s)], thus supporting our simple analysis.

Hence, our transport data collected on Co/LAO/STO heterostructures clearly indicate the presence of an electronic system at the LAO/STO interface whose behavior is very similar to the usual LAO($n \geq 4$ uc)/STO, even for LAO as thin as a single uc. Furthermore, the estimated carrier densities (several 10^{13} to 1×10^{14} cm^{-2}) in Co/LAO/STO samples are comparable to values typically found for quasi-two-dimensional electronic systems (q-2DES) at LAO/STO interfaces[3,23,24].

X-ray absorption spectroscopy.

To gain further insight into the electronic structure of Co/LAO/STO systems, we have performed X-ray absorption spectroscopy (XAS) measurements at the DEIMOS beamline of Synchrotron SOLEIL. XAS probes transitions from core electronic states to excited electronic states. The energy of the incident X-ray beam can be tuned to the Ti $L_{2,3}$ absorption edge to probe electronic transitions from $2p_{3/2}$ and $2p_{1/2}$ to $3d$ levels [see Fig. 3(a)][25]. Therefore, the preferential occupancy of states with different orbital symmetries can be probed by X-ray linear dichroism (XLD), that is the difference in XAS measured with a linear horizontal (LH) or vertical (LV) polarization of the X-ray beam [see Fig. 3(b)], *i.e.* XLD = (LH - LV). Conversely, the isotropic signal is defined as the mean of the two: ISO = (LH + LV)/2.

The XAS experiments were performed at the Ti $L_{2,3}$ absorption edge, on the same Co/LAO(n=0,2 uc)/STO samples previously shown in Figures 1 and 2, as well as on a bare STO substrate, on insulating LAO(2 uc)/STO and on a conducting LAO(4 uc)/STO sample. All spectra were collected at 300 K in total electron yield (TEY) mode in order to be surface sensitive. On Figure 3, the ISO signal appears for all samples to be largely of Ti^{4+} character[26]. The XLD signals however display significant differences between the samples [see Fig. 3(d)]. In LAO/STO samples with 2 and 4 uc of LAO, the XLD shows a sign reversal with respect to that obtained from a bare STO substrate. This is related to an inverted (negative *vs.* positive) splitting of the $3d$ bands [see Fig. 3(f)]. Interestingly, the XLD measured on the Co/LAO(2 uc)/STO sample is also very different from that of the STO substrate and appears very similar to the uncapped LAO/STO samples. Although much more noisy, the XLD signal of the Co/STO sample resembles that of the bare STO.

In bulk cubic STO, the crystal field splits the five-fold degenerate Ti $3d$ bands into 2-fold e_g ($d_{x^2-y^2}$, d_{z^2}) and 3-fold t_{2g} (d_{xy}, d_{xz}, d_{yz}) degenerate bands[27]. In an attempt to clarify this band picture, we have performed atomic multiplet calculations using the CTM4XAS program[28]. It allowed us to explore the effect of a symmetry reduction of the system (*e.g.* toward tetragonal), which distorts the TiO_6 octahedra and lifts the degeneracy of the e_g and t_{2g} bands [see Fig. 3(e,f)]. The measured XLD were well reproduced by using values of the energy splittings identical to those reported in the literature. In the case of STO, we considered *positive* energy splittings Δe_g = 40 meV

and $\Delta t_{2g} = 25$ meV [29]. In contrast, for the LAO/STO and Co/LAO/STO systems, *negative* energy splittings $\Delta e_g = -100$ meV and $\Delta t_{2g} = -50$ meV were considered[30]. We note that introducing a Co capping layer does not alter the fine structure of the XLD observed in uncovered LAO/STO samples. Interestingly, we have shown that Co-capped and uncapped LAO/STO systems have a similar subband structure, with a preferential d_{xy} orbital occupancy.

Incidentally, we performed X-ray magnetic circular dichroism (XMCD) experiments at the Ti $L_{2,3}$ edge on Co/LAO(n)/STO samples with $n = 2$ and 4 uc samples (see Supplementary Information). The signal-to-noise ratio of our experiments allows us to estimate the Ti magnetic moment averaged over the total probing depth to be of the order of 10^{-2} μ_B/atom. This value is in agreement with those obtained from the DFT calculations presented below as well as from neutron reflectometry on LAO/STO superlattices[31] and recent XMCD experiments on similarly prepared LAO/STO conducting interfaces[32].

First-principles calculations.

To elucidate the origin of the observed onset of conductivity below four unit cells of LAO, DFT calculations were performed on Co(m)/LAO(n)/STO(001). We used the all-electron full-potential linearized augmented plane wave (FP-LAPW), as implemented in the WIEN2k code[33,34]. For the exchange-correlation functional we used the generalized gradient approximation (GGA)[35]. The influence of electronic correlations beyond GGA are discussed in the Supplementary Information. The in-plane lattice parameter is set to the GGA equilibrium lattice constant of STO ($a_{\mathrm{STO}} = 3.92$ Å) and the atomic positions are fully relaxed within tetragonal symmetry. More details are provided in Ref. 18 and Supplementary Information. Figure 4(a) shows the layer resolved density of states (LDOS) of a (001)-oriented STO substrate (4.5 uc thick) covered with one monolayer (ML) of Co. In contrast to the uncovered STO(001) substrate (not shown here), where the Fermi level is pinned at the top of the valence band defined by surface states at the topmost TiO_2 layer, for Co/STO(001) E_{F} shifts to the bottom of the Ti conduction band, leaving the Ti 3d band empty.

In the uncovered LAO(1 uc)/STO system, the Fermi level lies at the top of the valence band [Fig. 4(b), determined by O 2p states of the surface AlO_2 layer, while the conduction band minimum is 2 eV above the Fermi energy (E_{F}) and is determined by Ti 3d states. Adding a Co capping layer shifts the Fermi level to the bottom of the conduction band in Co/LAO(1 uc)/STO [Fig. 4(c)]. In contrast to LAO(1 uc)/STO and to Co/STO, in Co/LAO(1 uc)/STO the Ti 3d band is now partially occupied, with a small spin polarization of -0.02 to -0.03μ_B per Ti. In Co/LAO/STO samples, a metallic bilayer is hence formed with a conducting surface (Co) and a conducting burried interface (STO side), consistent with the transport data. Furthermore, the Ti 3d band occupation increases weakly with LAO thickness (Supplementary Information). Adding the Co capping layer (largely) cancels the internal potential buildup within the polar LAO film. As found previously[18], the position of the Fermi level with respect to the conduction band minimum in STO is determined by the work function of the metallic contact (4.72 eV for 1 ML Co and 4.28 eV for 3 ML Co). This, together with the still persisting polar discontinuity at the LAO/STO interface leads to a finite occupation of the Ti 3d band at the interface.

Next, we explore the preferential orbital occupancy of the electronic system. The electron density of Co/LAO(1 uc)/STO, integrated between $E_{\mathrm{F}} - 0.50$ eV and E_{F} reveals predominant d_{xy} orbital polarization of Ti in the interface layer and

d_{xz}/d_{yz} character in deeper layers [see Fig. 4(d)], which can also be seen on the projected density of states in Fig. 4(e). To confirm the picture proposed in Fig. 3(e,f), we have analyzed the structural distortions of the octahedra within the Co/LAO(1 uc)/STO heterostructure. We find that the average distance between the apical oxygens on both sides of Ti in the [001] direction is 3.92Å for the interfacial (IF) and 3.99Å for the IF-1 layers, respectively. In line with the experimentally determined t_{2g} splittings [Fig. 3(d-f)], we find that a shortened (expanded) TiO_6 octahedra average size in the [001] direction corresponds to d_{xy} orbitals lying lower (higher) in energy.

DISCUSSION

Using four points transport experiments, we have revealed the presence of metallic conduction at the $LaAlO_3/SrTiO_3$ interface for $Co/LaAlO_3(n)/SrTiO_3$ heterostructures with $LaAlO_3$ thicknesses 1 uc $\leq n \leq$ 4 uc. The linear dichroism observed through X-ray absorption spectroscopy evidences a compressive tetragonal distortion of the TiO_6 octahedra for cobalt-capped and uncapped $LaAlO_3/SrTiO_3$ systems. Making use of atomic multiplet calculations we found that in $Co/LaAlO_3/SrTiO_3$ the Ti orbitals reconstruct from the situation in bare $SrTiO_3$ substrates. As a result, the lowest energy level has a d_{xy} orbital character for $Co/LaAlO_3/SrTiO_3$ systems, compared to d_{xz}/d_{yz} for the bare $SrTiO_3$. DFT calculations support this picture and predict structural distortions that agree with those inferred from XAS. Further, they indicate a finite occupancy of the Ti d bands at the Fermi energy for the $Co/LaAlO_3$(1 uc)$/SrTiO_3$ heterostructure, with a predominant d_{xy} orbital character within the interfacial TiO_2 layer. The metallic Co overlayer thus appears to modify the electrostatic boundary conditions of the LAO/STO system, leading to the occupation of the Ti 3d bands. These observations support the electrostatic origin of the q-2DES at the LAO/STO interface as proposed in the polar catastrophe model[17,36], which suggests that cationic intermixing across the interface[37] or oxygen vacancies[38–40] only play a marginal role.

For spintronics and tunneling spectroscopy applications, it is necessary to control the tunnel barrier resistance, which is usually achieved by tuning its thickness. In the $LaAlO_3/SrTiO_3$ case, a stringent limitation for efficient tunneling was the existence of a minimum thickness of 4 unit cells of $LaAlO_3$ for the onset of conductivity. Our findings should therefore considerably facilitate spin injection[41,42] or tunnel spectroscopy studies[43–45] only achievable in perpendicular geometries, thereby paving the way toward $LaAlO_3/SrTiO_3$-based electronic and spintronic tunneling devices with tunable tunnel resistances.

METHODS

Samples fabrication

The $LaAlO_3$ (LAO) films were grown by pulsed laser deposition (PLD) on 5×5 mm^2 TiO_2-terminated (001)-oriented $SrTiO_3$ (STO) substrates. A single crystal LAO target was ablated by a KrF (248 nm) excimer laser at a repetition rate of 1 Hz and with a fluence of approximately 1 J·cm^{-2}. The LAO deposition was performed in an oxygen partial pressure of 2.0×10^{-4} mbar and at a substrate temperature of 730°C. Substrate-to-target distance was 63 mm. The layer-by-layer growth mode allowed us to precisely control the LAO thickness through real time monitoring of reflection high-energy electron diffraction (RHEED) intensity oscillations (5). The samples were then

annealed for 30 minutes in about 400 mbar of oxygen at 500°C[38,39]. Finally, the LAO/STO heterostructures were cooled at 25°C/minute and kept in the same oxygen pressure for approximately 30 to 60 minutes. PLD growth was followed by *in situ* deposition of a metallic cobalt electrode by magnetron sputtering at room temperature in a pure Ar atmosphere of 4.5×10^{-4} mbar, resulting in a clean Co/LAO interface. The 2 to 2.5 nm Co thin films were capped with a 3 nm AlO_x layer to prevent cobalt oxidation. For the Co/STO sample, the same procedure of thermal and pressure cycles as the one described above were applied to the TiO_2-terminated STO substrate, minus the LAO deposition step, prior the Co deposition.

Density Functional Theory Calculations

DFT calculations were performed on Co(m)/LAO(n)/STO(001) using the all-electron full-potential linearized augmented plane wave (FP-LAPW) method, as implemented in the WIEN2k code[33,34]. For the exchange-correlation potential we used the generalized gradient approximation (GGA)[35]. The muffin-tin spheres of the atoms were taken as: 2.3, 1.8, and 1.6 a.u. for La/Sr, Ti/Co/Al, and O, respectively. The energy cutoff for the plane wave representation in the interstitial is $E^{wf}_{max} = 19\,\mathrm{Ry}$ for the wave functions. The spherical harmonics inside the muffin-tin spheres are expanded up to $l_{max} = 10$, while the plane wave expansion of the charge density was truncated at $G_{max} = 12\,(\mathrm{a.u.})^{-1}$. The integrals over the Brillouin zone are performed with 36 k-points in the irreducible part of the Brillouin zone (IBZ) using the Monkhorst-Pack special k-points approach[46]. We have chosen a symmetric slab with LAO and Co layers on both sides of the 4.5 uc thick STO substrate and a vacuum region between the slab and its periodic images of at least 10 Å. The Co atoms are adsorbed on top of the oxygen ions at the surface of TiO_2 or AlO_2. The in-plane lattice parameter is set to the GGA equilibrium lattice constant of STO ($a_{\mathrm{STO}} = 3.92\,\mathrm{Å}$) and the atomic positions are fully relaxed within tetragonal symmetry.

REFERENCES

[1] Hwang, H. Y., Iwasa, Y., Kawasaki, M., Keimer, B., Nagaosa, N., and Tokura, Y. Emergent phenomena at oxide interfaces. *Nat. Mater.* **11,** 103–13 (2012).

[2] Ohtomo, A. and Hwang, H. Y. A high-mobility electron gas at the $LaAlO_3/SrTiO_3$ heterointerface. *Nature* **427,** 423–6 (2004).

[3] Thiel, S., Hammerl, G., Schmehl, A., Schneider, C. W., and Mannhart, J. Tunable quasi-two-dimensional electron gases in oxide heterostructures. *Science* **313,** 1942–5 (2006).

[4] Ben Shalom, M., Sachs, M., Rakhmilevitch, D., Palevski, A., and Dagan, Y. Tuning spin-orbit coupling and superconductivity at the $SrTiO_3/LaAlO_3$ interface: A magnetotransport study. *Phys. Rev. Lett.* **104,** 126802 (2010).

[5] Caviglia, A. D., Gabay, M., Gariglio, S., Reyren, N., Cancellieri, C., and Triscone, J.-M. Tunable Rashba spin-orbit interaction at oxide interfaces. *Phys. Rev. Lett.* **104,** 126803 (2010).

[6] Reyren, N., Thiel, S., Caviglia, A. D., Kourkoutis, L. F., Hammerl, G., Richter, C., Schneider, C. W., Kopp, T., Rüetschi, A.-S., Jaccard, D., Gabay, M., Muller, D. A., Triscone, J.-M., and Mannhart, J. Superconducting interfaces between insulating oxides. *Science* **317,** 1196–9 (2007).

[7] Caviglia, A. D., Gariglio, S., Reyren, N., Jaccard, D., Schneider, T., Gabay, M., Thiel, S., Hammerl, G., Mannhart, J., and Triscone, J.-M. Electric field control of the $LaAlO_3/SrTiO_3$ interface ground state. *Nature* **456,** 624–7 (2008).

[8] Bell, C., Harashima, S., Kozuka, Y., Kim, M., Kim, B. G., Hikita, Y., and Hwang, H. Y. Dominant mobility modulation by the electric field effect at the $LaAlO_3/SrTiO_3$ interface. *Phys. Rev. Lett.* **103,** 226802 (2009).

[9] Brinkman, A., Huijben, M., van Zalk, M., Huijben, J., Zeitler, U., Maan, J. C., van der Wiel, W. G., Rijnders, G., Blank, D. H. A., and Hilgenkamp, H. Magnetic effects at the interface between non-magnetic oxides. *Nat. Mater.* **6,** 493–6 (2007).

[10] Ariando, Wang, X., Baskaran, G., Liu, Z. Q., Huijben, J., Yi, J. B., Annadi, A., Barman, A. R., Rusydi, A., Dhar, S., Feng, Y. P., Ding, J., Hilgenkamp, H., and Venkatesan, T. Electronic phase separation at the $LaAlO_3/SrTiO_3$ interface. *Nat. Commun.* **2,** 188 (2011).

[11] Bert, J. A., Kalisky, B., Bell, C., Kim, M., Hikita, Y., Hwang, H. Y., and Moler, K. A. Direct imaging of the coexistence of ferromagnetism and superconductivity at the $LaAlO_3/SrTiO_3$ interface. *Nat. Phys.* **7,** 767–771 (2011).

[12] Dikin, D. A., Mehta, M., Bark, C. W., Folkman, C. M., Eom, C. B., and Chandrasekhar, V. Coexistence of superconductivity and ferromagnetism in two dimensions. *Phys. Rev. Lett.* **107,** 056802 (2011).

[13] Li, L., Richter, C., Mannhart, J., and Ashoori, R. C. Coexistence of magnetic order and two-dimensional superconductivity at $LaAlO_3/SrTiO_3$ interfaces. *Nat. Phys.* **7,** 762–766 (2011).

[14] Cen, C., Thiel, S., Mannhart, J., and Levy, J. Oxide nanoelectronics on demand. *Science* **323,** 1026–30 (2009).

[15] Li, L., Richter, C., Paetel, S., Kopp, T., Mannhart, J., and Ashoori, R. C. Very large capacitance enhancement in a two-dimensional electron system. *Science* **332,** 825–828 (2011).

[16] Förg, B., Richter, C., and Mannhart, J. Field-effect devices utilizing $LaAlO_3$-$SrTiO_3$ interfaces. *Appl. Phys. Lett.* **100,** 053506 (2012).

[17] Nakagawa, N., Hwang, H. Y., and Muller, D. A. Why some interfaces cannot be sharp. *Nat. Mater.* **5,** 204–209 (2006).

[18] Arras, R., Ruiz, V. G., Pickett, W. E., and Pentcheva, R. Tuning the two-dimensional electron gas at the $LaAlO_3/SrTiO_3(001)$ interface by metallic contacts. *Phys. Rev. B* **85,** 125404 (2012).

[19] van der Pauw, L. A method of measuring the resistivity and Hall coefficient on lamellae of arbitrary shape. *Philips Tech. Rev.* **20,** 220–224 (1958).

[20] Popović, Z., Satpathy, S., and Martin, R. Origin of the two-dimensional electron gas carrier density at the $LaAlO_3$ on $SrTiO_3$ Interface. *Phys. Rev. Lett.* **101,** 256801 (2008).

[21] Pentcheva, R., Huijben, M., Otte, K., Pickett, W. E., Kleibeuker, J. E., Huijben, J., Boschker, H., Kockmann, D., Siemons, W., Koster, G., Zandvliet, H. J. W., Rijnders, G., Blank, D. H. A., Hilgenkamp, H., and Brinkman, A. Parallel electron-hole bilayer conductivity from electronic interface reconstruction. *Phys. Rev. Lett.* **104,** 166804 (2010).

[22] Joshua, A., Pecker, S., Ruhman, J., Altman, E., and Ilani, S. A universal critical density underlying the physics of electrons at the $LaAlO_3/SrTiO_3$ interface. *Nat. Commun.* **3,** 1129 (2012).

[23] Caviglia, A. D., Gariglio, S., Cancellieri, C., Sacépé, B., Fête, A., Reyren, N., Gabay, M., Morpurgo, A. F., and Triscone, J.-M. Two-dimensional quantum oscillations of the conductance at $LaAlO_3/SrTiO_3$ interfaces. *Phys. Rev. Lett.* **105,** 236802 (2010).

[24] Ben Shalom, M., Ron, A., Palevski, A., and Dagan, Y. Shubnikov-De Haas Oscillations in $SrTiO_3/LaAlO_3$ Interface. *Phys. Rev. Lett.* **105,** 206401 (2010).

[25] Cowan, R. D. *The Theory of Atomic Structure and Spectra.* (University of California Press, Berkeley, 1981).

[26] de Groot, F. M. F., Fuggle, J., Thole, B., and Sawatzky, G. L2,3 x-ray-absorption edges of d0 compounds: K+, Ca2+, Sc3+, and Ti4+ in Oh (octahedral) symmetry. *Phys. Rev. B* **41,** 928–937 (1990).

[27] Mattheiss, L. Energy bands for $KNiF_3$, $SrTiO_3$, $KMoO_3$, and $KTaO_3$. *Phys. Rev. B* **6,** 4718–4740 (1972).

[28] Stavitski, E. and de Groot, F. M. F. The CTM4XAS program for EELS and XAS spectral shape analysis of transition metal L edges. *Micron* **41,** 687 (2010).

[29] Salluzzo, M., Gariglio, S., Torrelles, X., Ristic, Z., Di Capua, R., Drnec, J., Sala, M. M., Ghiringhelli, G., Felici, R., and Brookes, N. B. Structural and electronic reconstructions at the $LaAlO_3/SrTiO_3$ interface. *Adv. Mater.* **25,** 2333–2338 (2013).

[30] Salluzzo, M., Cezar, J., Brookes, N., Bisogni, V., De Luca, G., Richter, C., Thiel, S., Mannhart, J., Huijben, M., Brinkman, A., Rijnders, G., and Ghiringhelli, G. Orbital reconstruction and the two-dimensional electron gas at the $LaAlO_3/SrTiO_3$ interface. *Phys. Rev. Lett.* **102,** 166804 (2009).

[31] Fitzsimmons, M., Hengartner, N., Singh, S., Zhernenkov, M., Bruno, F., Santamaria, J., Brinkman, A., Huijben, M., Molegraaf, H., de la Venta, J., and Schuller, I. Upper limit to magnetism in $LaAlO_3/SrTiO_3$ heterostructures. *Phys. Rev. Lett.* **107,** 217201 (2011).

[32] Salluzzo, M., Gariglio, S., Stornaiuolo, D., Sessi, V., Rusponi, S., Piamonteze, C., De Luca, G. M., Minola, M., Marré, D., Gadaleta, A., Brune, H., Nolting, F., Brookes, N. B., and Ghiringhelli, G. Origin of interface magnetism in $BiMnO_3/SrTiO_3$ and $LaAlO_3/SrTiO_3$ heterostructures. *Phys. Rev. Lett.* **111,** 087204 (2013).

[33] Schwarz, K. and Blaha, P. Solid state calculations using wien2k. *Computational Materials Science* **28,** 259–273 (2003).

[34] Blaha, P., Schwarz, K., Madsen, G. K. H., Kvasnicka, D., and Luitz, J. *WIEN2k, An Augmented Plane Wave Plus Local Orbitals Program for Calculating Crystal Properties*. (Vienna University of Technology, Vienna, Austria, 2001).

[35] Perdew, J. P., Burke, K., and Ernzerhof, M. Generalized gradient approximation made simple. *Phys. Rev. Lett.* **77,** 3865–3868 (1996).

[36] Reinle-Schmitt, M. L., Cancellieri, C., Li, D., Fontaine, D., Medarde, M., Pomjakushina, E., Schneider, C., Gariglio, S., Ghosez, P., Triscone, J.-M., and Willmott, P. Tunable conductivity threshold at polar oxide interfaces. *Nat. Commun.* **3,** 932 (2012).

[37] Willmott, P., Pauli, S., Herger, R., Schlepütz, C., Martoccia, D., Patterson, B., Delley, B., Clarke, R., Kumah, D., Cionca, C., and Yacoby, Y. Structural basis for the conducting interface between $LaAlO_3$ and $SrTiO_3$. *Phys. Rev. Lett.* **99,** 155502 (2007).

[38] Cancellieri, C., Reyren, N., Gariglio, S., Caviglia, A. D., Fête, A., and Triscone, J.-M. Influence of the growth conditions on the $LaAlO_3/SrTiO_3$ interface electronic properties. *EPL (Europhys. Lett.)* **91,** 17004 (2010).

[39] Basletic, M., Maurice, J.-L., Carrétéro, C., Herranz, G., Copie, O., Bibes, M., Jacquet, E., Bouzehouane, K., Fusil, S., and Barthélémy, A. Mapping the spatial distribution of charge carriers in $LaAlO_3/SrTiO_3$ heterostructures. *Nat. Mater.* **7,** 621–625 (2008).

[40] Liu, Z. Q., Li, C. J., Lü, W. M., Huang, X. H., Huang, Z., Zeng, S. W., Qiu, X. P., Huang, L. S., Annadi, A., Chen, J. S., Coey, J. M. D., Venkatesan, T., and Ariando. Origin of the two-dimensional electron gas at $LaAlO_3/SrTiO_3$ interfaces: The role of oxygen vacancies and electronic reconstruction. *Phys. Rev. X* **3,** 021010 (2013).

[41] Fert, A. and Jaffrès, H. Conditions for efficient spin injection from a ferromagnetic metal into a semiconductor. *Phys. Rev. B* **64,** 184420 (2001).

[42] Reyren, N., Bibes, M., Lesne, E., George, J.-M., Deranlot, C., Collin, S., Barthélémy, A., and Jaffrès, H. Gate-controlled spin injection at $LaAlO_3/SrTiO_3$ interfaces. *Phys. Rev. Lett.* **108,** 186802 (2012).

[43] Breitschaft, M., Tinkl, V., Pavlenko, N., Paetel, S., Richter, C., Kirtley, J. R., Liao, Y. C., Hammerl, G., Eyert, V., Kopp, T., and Mannhart, J. Two-dimensional electron liquid state at $LaAlO_3/SrTiO_3$ interfaces. *Phys. Rev. B* **81,** 153414 (2010).

[44] Ristic, Z., Di Capua, R., Chiarella, F., De Luca, G. M., Maggio-Aprile, I., Radovic, M., and Salluzzo, M. Photodoping and in-gap interface states across the metal-insulator transition in $LaAlO_3/SrTiO_3$ heterostructures. *Phys. Rev. B* **86,** 045127 (2012).

[45] Richter, C., Boschker, H., Dietsche, W., Fillis-Tsirakis, E., Jany, R., Loder, F., Kourkoutis, L. F., Muller, D. A., Kirtley, J. R., Schneider, C. W., and Mannhart, J. Interface superconductor with gap behaviour like a high-temperature superconductor. *Nature* **502,** 528–31 (2013).

[46] Monkhorst, H. J. and Pack, J. D. Special points for brillouin-zone integrations. *Phys. Rev. B* **13,** 5188–5192 (1976).

ACKNOWLEDGMENTS

We acknowledge fruitful discussions with C. Deranlot. We would like to thank E. Jacquet for his support with the PLD and sputtering systems, and D. Sando for a careful reading of the manuscript. We acknowledge SOLEIL for provision of synchrotron radiation facilities (project No. 20111079). This Work was partly supported by the European Research Council (ERC Advanced Grant FEMMES, No. 267579), the German Science Foundation through project C3 within SFB/TR80 and grant h0721 for computational time at the supercomputers of the Leibniz Rechnenzentrum, Garching.

AUTHOR CONTRIBUTIONS

A.B. and M.B. supervised the project. E.L. and N.R. fabricated the samples, performed and analysed the transport measurements. E.L., N.R., R.M., F.C., V.C., P.O. and A.B. performed synchrotron measurements. E.L., N.R., R.M. and P.O. analysed the synchrotron data. D.D. and R.P. performed the ab-initio calculations. All authors contributed to interpretation of the results. E.L., N.R., D.D. and R.P. wrote the manuscript with inputs from P.O. and M.B.

ADDITIONAL INFORMATION

Competing financial interests:

The authors declare no competing financial interests.

FIG. 1. **Sheet resistances as a function of temperature.** (a) Measured longitudinal resistance R_{xx}^{meas} *vs.* temperature T of LAO(4 uc)/STO and Co/LAO(n)/STO samples showing a clear metallic behavior. The Co/STO resistance remains almost unchanged from 300 K to 1.4 K ($\Delta R < 1\%$). Inset: Measurement configuration. (b) Calculated sheet resistance $R_{\square}^{STO}$ of the conducting STO sublayer in Co/LAO(n)/STO samples (according to Eq. 1), and measured sheet resistance of the LAO(4 uc)/STO samples. The blue dotted line corresponds to the Co/STO data set.

FIG. 2. **Hall measurements.** (a) Antisymmetrized Hall resistance R_{xy} as a function of applied magnetic field $\mu_0 H$ for an LAO(4 uc)/STO sample displaying a linear Hall effect at room temperature. Inset: R_{xy} *vs.* $\mu_0 H$ for various Co/LAO(n)/STO samples at 290 K showing cobalt dominated AHE at low magnetic field. (b) Antisymmetrized Hall resistance R_{xy} *vs.* $\mu_0 H$ of an LAO(4 uc)/STO sample and of Co/LAO(n)/STO at 1.4 K. Inset: R_{xy} *vs.* $\mu_0 H$ for Co/STO at 1.4 K similar to the one observed at 290 K.

FIG. 3. **X-ray absorption spectroscopy at Ti L edge.** (a) Sketch of the X-ray absorption spectroscopy (XAS) process depicting the $2p \rightarrow 3d$ electronic transitions at the Ti $L_{2,3}$ edge. (b) Scheme of the XAS measurement geometries with linearly horizontal (LH) and linearly vertical (LV) polarized light. The incident beam forms a 30° angle with the sample surface (x,y). (c) Experimentally measured isotropic signals (ISO) *vs.* photon energy of a STO(001) substrate, and of various (Co/)LAO(n)/STO samples. Spectra acquired at 300 K in TEY mode. (d) The corresponding experimental X-ray linear dichroism (XLD) signals show a sign inversion between the XLD of STO and Co/STO and that of LAO(2,4 uc) and Co/LAO(2 uc) samples. (e) Calculated XLD which reproduces the experimental XLD of the STO bare substrate (circle, [A]) and of the Co/LAO(2 uc)/STO sample (square, [B]). (f) The cubic crystal field (CF) splits the Ti^{4+} $3d$ states into e_g and t_{2g} levels. A tetragonal CF further lifts the orbital degeneracy, with: [A] case of STO, [B] case of (Co/)LAO/STO.

FIG. 4. **Layer-resolved density of states (LDOS).** (a) Co(1 ML)/STO, (b) LAO(1 uc)/STO, and (c) Co(1 ML)/LAO(1 uc)/STO heterostructures within GGA with a 4.5 uc thick STO substrate. (d) Side view of Co(1 ML)/LAO(1 uc)/STO with the electron density integrated in the interval $E_F - 0.50$ eV to E_F, giving insight into the Ti $3d$ orbital occupation. (e) Projected density of states (PDOS) of Ti in the interface (IF) and IF-1 layer of Co/LAO(1 uc)/STO. Positive (negative) values correspond to majority (minority) spin. $E = 0$ eV corresponds to the Fermi level.

FIG. 5. ***In situ*** **RHEED characterisation.** (a) Monitoring of the RHEED (01) diffraction peak intensity *vs.* time during the epitaxial growth of LAO films of various thicknesses (1 to 4 uc) on STO substrates. Inset: Typical RHEED pattern of (b) an STO substrate, (c) a 4 uc LAO thin film on STO, taken at 730°C in an oxygen partial pressure of 2.0×10^{-4} mbar. Arrows indicate the end of the growth. Asterisks designate samples later covered with a Co/AlO_x capping.

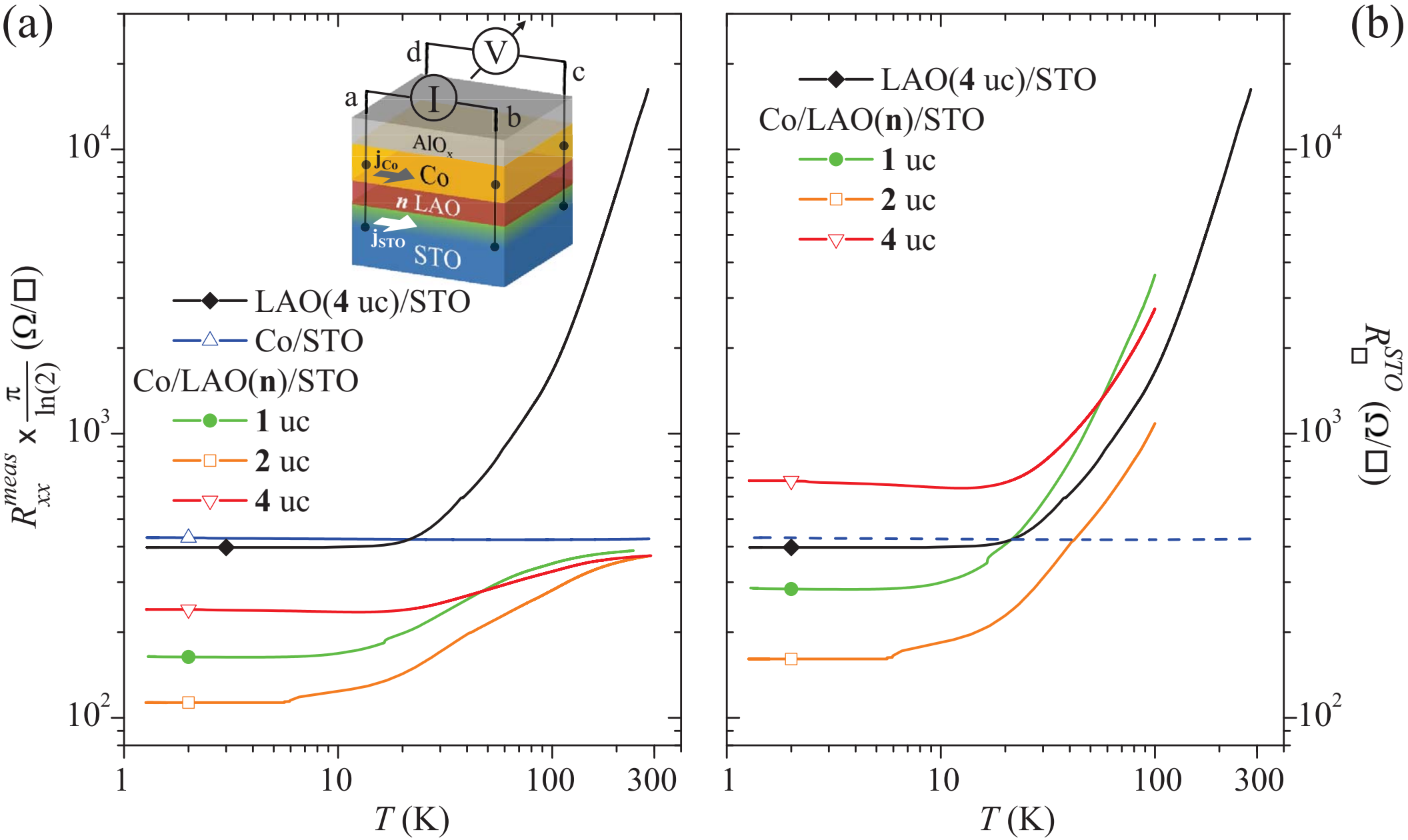
(a)
(b)
d
V
c
a
I
b
AlO$_x$
j_{Co}
Co
n LAO
j_{STO}
STO
LAO(**4** uc)/STO
Co/STO
Co/LAO(**n**)/STO
1 uc
2 uc
4 uc
$R_{xx}^{meas} \times \frac{\pi}{\ln(2)}$ (Ω/□)
$R_{\square}^{STO}$ (Ω/□)
10^4
10^3
10^2
1
10
100
300
T (K)

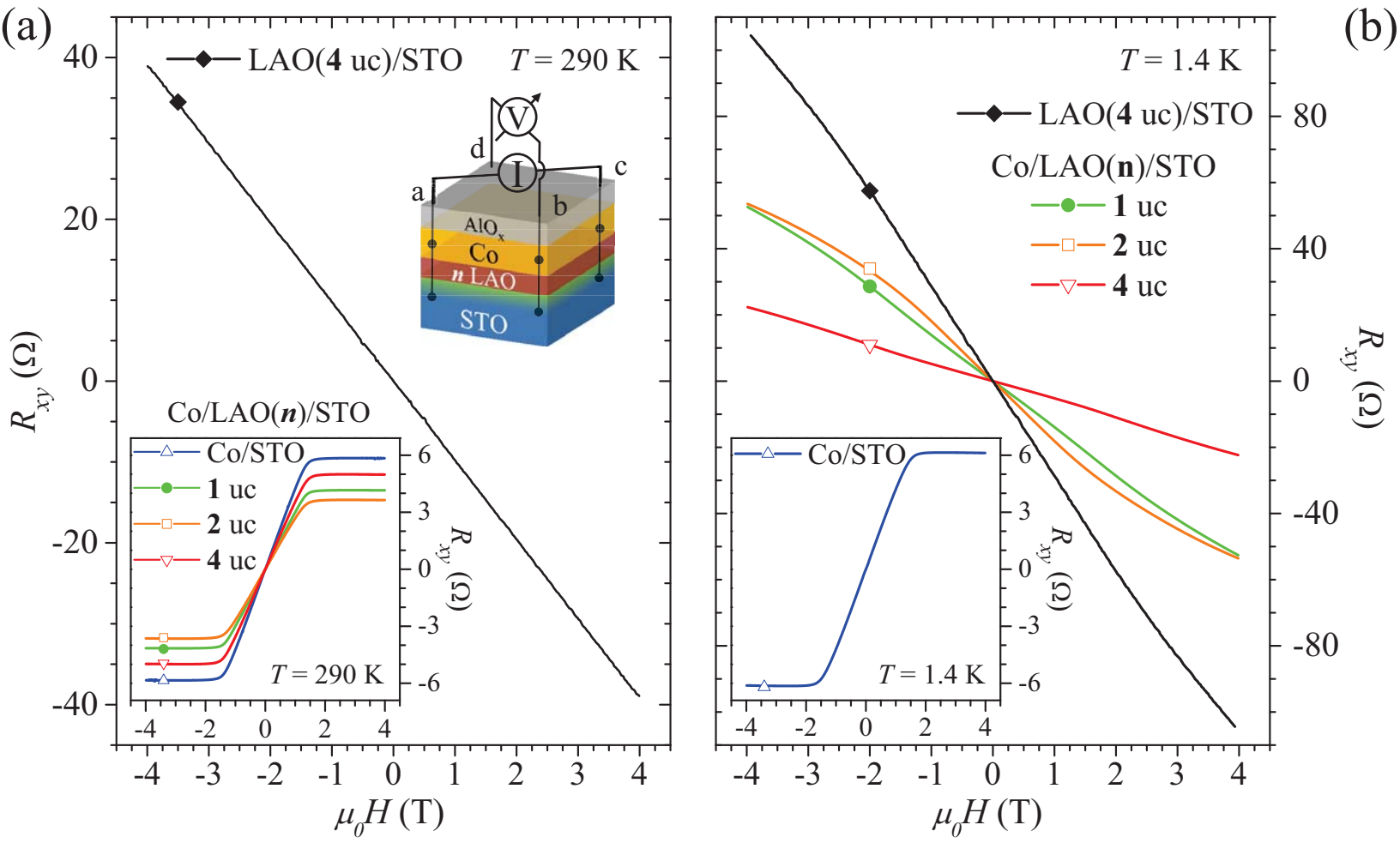
(a)
LAO(4 uc)/STO
T = 290 K
V
I
d
c
a
b
AlOx
Co
n LAO
STO
Co/LAO(n)/STO
Co/STO
1 uc
2 uc
4 uc
T = 290 K
Rxy (Ω)
μ0H (T)
(b)
T = 1.4 K
LAO(4 uc)/STO
Co/LAO(n)/STO
1 uc
2 uc
4 uc
Co/STO
T = 1.4 K
Rxy (Ω)
μ0H (T)

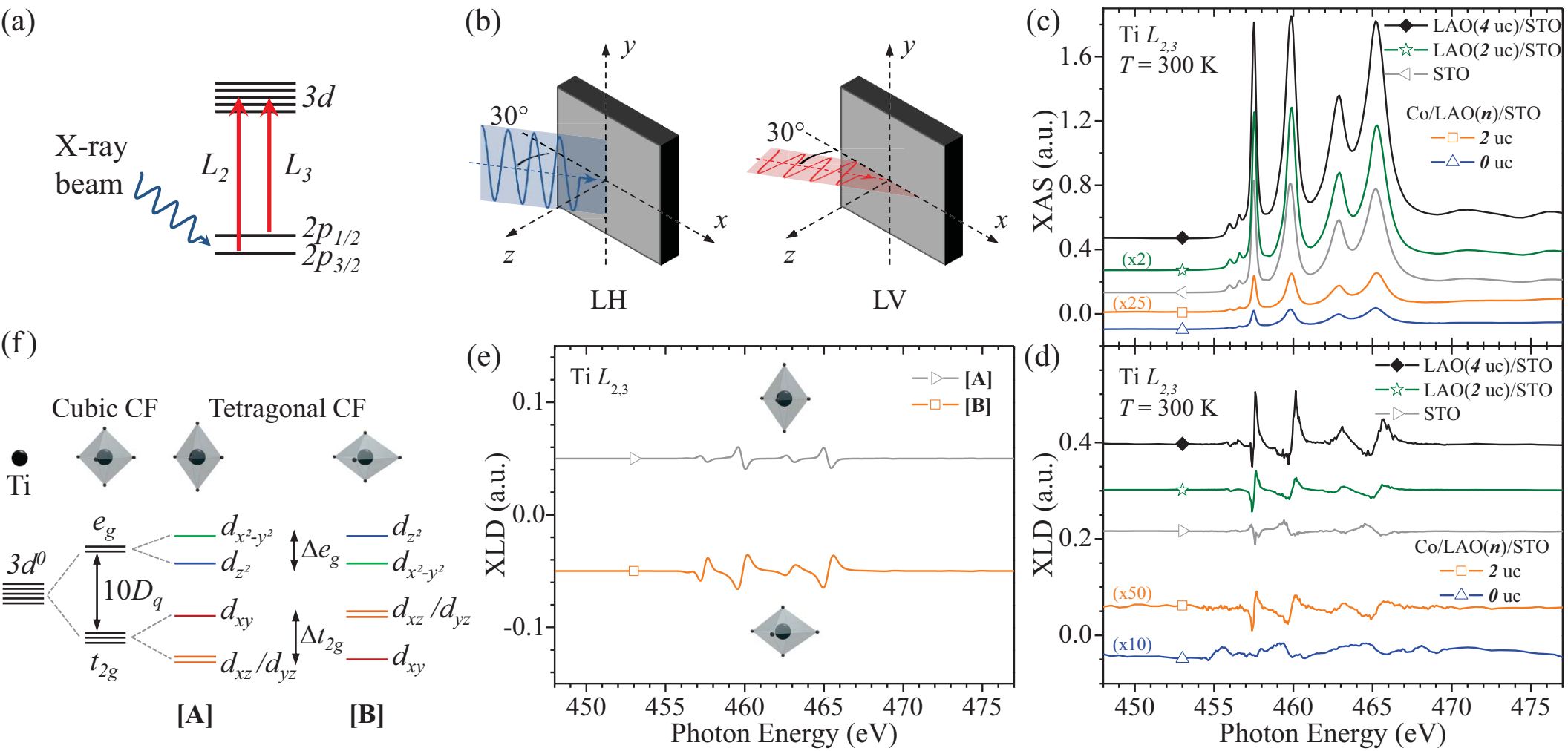
(a)
3d
X-ray beam
L2
L3
2p1/2
2p3/2
(b)
y
30°
x
z
LH
LV
(c)
Ti L2,3
T = 300 K
LAO(4 uc)/STO
LAO(2 uc)/STO
STO
Co/LAO(n)/STO
2 uc
0 uc
XAS (a.u.)
(x2)
(x25)
(d)
XLD (a.u.)
(x50)
(x10)
Photon Energy (eV)
(e)
[A]
[B]
(f)
Cubic CF
Tetragonal CF
Ti
3d0
eg
10Dq
t2g
Δeg
Δt2g
dx²-y²
dz²
dxy
dxz /dyz
[A]
[B]

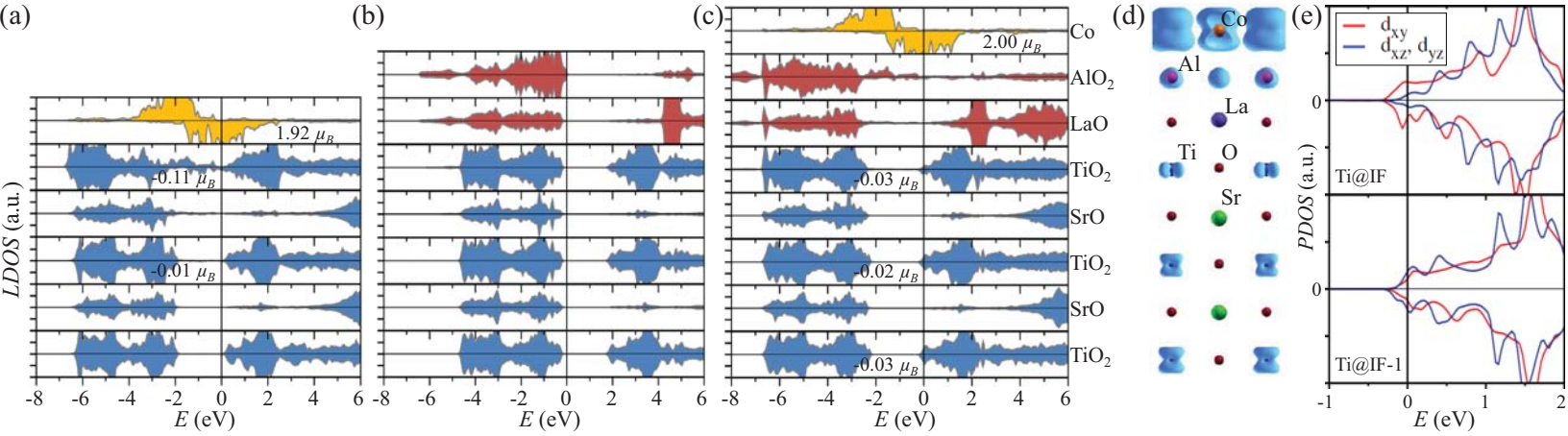
(a)
(b)
(c)
(d)
(e)
LDOS (a.u.)
E (eV)
1.92 μ_B
-0.11 μ_B
-0.01 μ_B
2.00 μ_B
-0.03 μ_B
-0.02 μ_B
-0.03 μ_B
Co
AlO_2
LaO
TiO_2
SrO
TiO_2
SrO
TiO_2
Al
La
Ti
O
Sr
Co
d_{xy}
d_{xz}, d_{yz}
PDOS (a.u.)
Ti@IF
Ti@IF-1

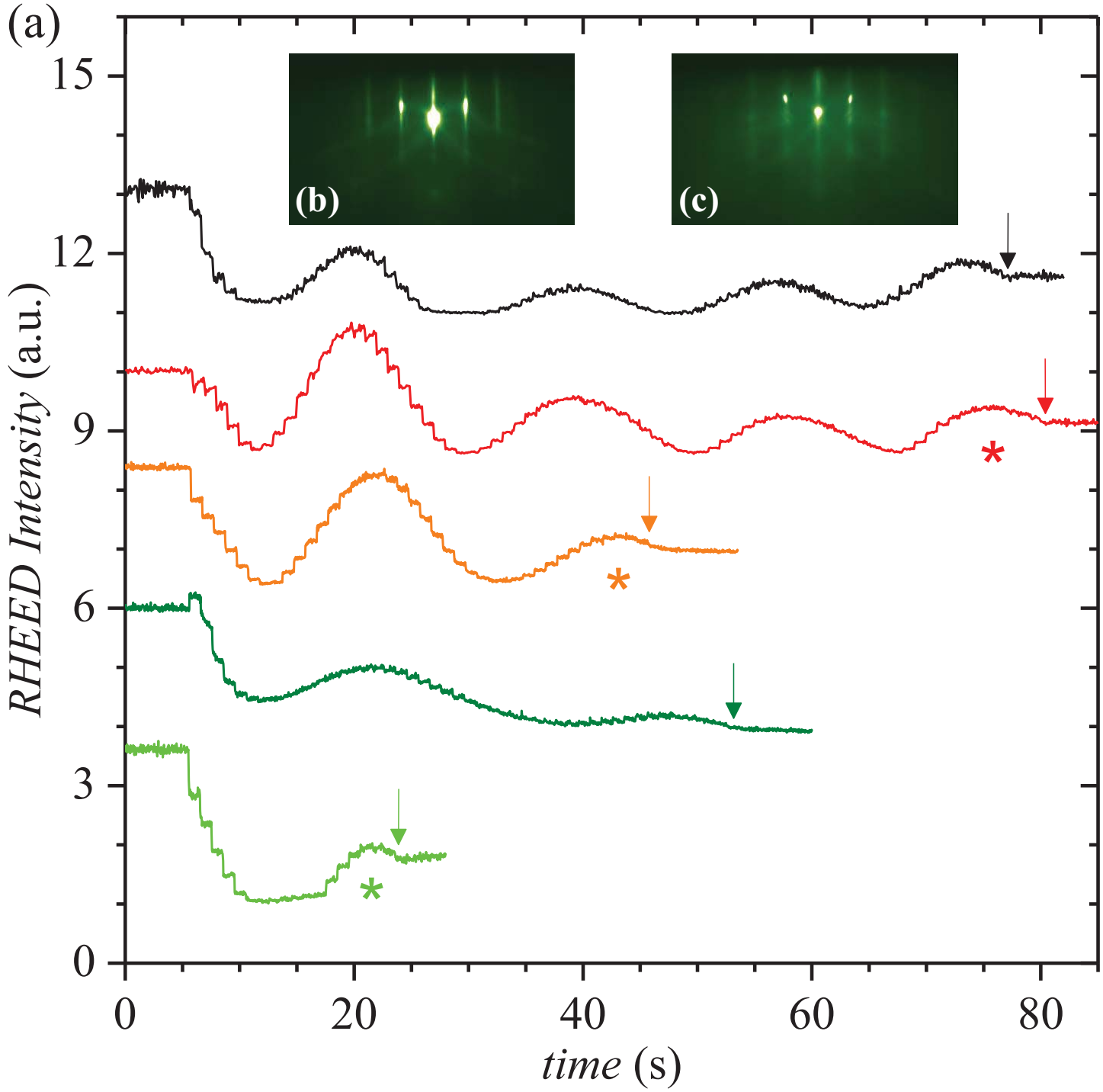
(a)
15
12
9
6
3
0
RHEED Intensity (a.u.)
0
20
40
60
80
time (s)
(b)
(c)
*
*
*